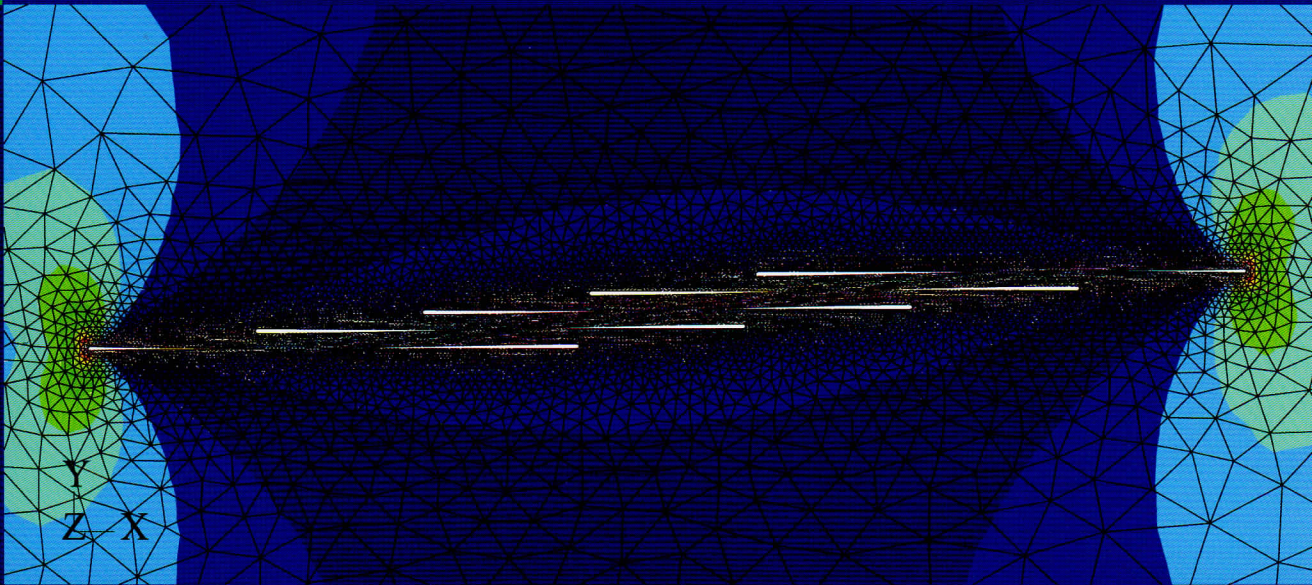


Friedrich G. Barth · Joseph A.C. Humphrey
Mandyam V. Srinivasan *Editors*

Frontiers in Sensing

From Biology to Engineering



Design and fabrication process for artificial lateral line sensors

28

Nima Izadi, Gijs J. M. Krijnen

Contents

| | | | |
|--|-----|---|-----|
| Abstract | 405 | 3. A capacitive sensor | 412 |
| 1. Introduction | 405 | 3.1 Analysis and design | 412 |
| 2. Piezoresistive sensors | 407 | 3.2 Fabrication | 415 |
| 2.1 Sensors based on cantilevers | 407 | 3.3 Distributed hair sensor array | 417 |
| 2.2 All polymer sensors | 411 | 3.4 Discussion | 417 |
| 2.3 Conclusion | 411 | 3.5 Conclusion | 419 |
| | | Summary | 419 |
| | | References | 419 |

Abstract

Biological sensory systems often display great performance, inspiring engineers to develop artificial counterparts. The lateral line system of fish has been widely studied by biologists for its crucial role in fish behaviour. Moreover recently the robustness, sensitivity and consequently wide range of applications that potentially benefit from the abilities of such a system have attracted the attention of the engineering community. Aquatic flow sensors based on the lateral line of fish are useful in underwater robotic applications for hydrodynamic imaging of complex and noisy environments to provide information for, for example, surveillance, navigation and obstacle detection. The speculative ability to manoeuvre in murky or dark water, especially object detection at short range, has strongly driven research in this area.

This chapter begins with a brief review of the state of the art flow sensors inspired by neuro-masts. Subsequently, the design principles and fabrication scheme for a differential capacitive flow sensor incorporating a hair-like structure are discussed. The main focus is on the application of Micro-Electro-Mechanical Systems (MEMS) technology, which enables fabrication of sensory structures on length-scales comparable to what can be found in nature. Its intrinsic batch fabrication capability and high spatial resolution facilitate the construction of dense arrays of flow sensors, eventually allowing the function of the fish lateral line to be copied.

1. Introduction

Aquatic environments have been the cradle of life ever since its earliest emergence on the planet. Fish, the inhabitants of the vast

Nima Izadi
University of Twente
Transducer Science and Technology
P.O. Box 217, 7500 AE Enschede, The Netherlands
e-mail: n.izadi@ewi.utwente.nl

oceans, have struggled through 530 millions years of existence and adapted to their resourceful but challenging surroundings. The need to perceive and locate prey and to escape from predators, or in general to survive in highly competitive situations, has driven such living organisms to develop various sensory organs. Whereas more well-known sensory systems, such as the visual system, have played their roles in sustaining life, fish and amphibians are in addition gifted with a sensory organ called the lateral line.

The lateral line system enables fish to use the velocity profile of the surrounding water to construct a 3D map of their immediate environment on which depends their ability to school, localise prey or predators and to avoid obstacles (Dijkgraaf 1963, Coombs 2001). In some species like the blind cave fish, which lacks visual capabilities, fish survival predominantly depends upon this system (von Campenhausen et al. 1981).

The lateral line system consists of mechanoreceptive hair cells, covered by a jelly-like cupula, which together are referred to as neuromasts. Neuromasts are either located on top of the skin at the bottom of a visible pit or groove (superficial neuromasts) or in the lateral line canals along the body (canal neuromasts). The displacement of the cupula due to fluid motion couples to the stereovilli of the hair cells and changes the firing rate of the afferent neurons (Voigt et al. 2000). Using this system, fish are able to perceive cupula displacements as small as a few nanometers which corresponds to a few

microns per second fluid velocity (van Netten 2006).

Man-made aquatic flow sensors have been built based on many sensing principles including heat conduction¹ (Chen and Liu 2003), the Doppler effect² (Jentink et al. 1987) and pressure difference³ (Fernandez et al. 2007), but they are still rarely utilized for underwater applications. Small, robust, cheap and low energy consuming sensors are needed in marine environments for numerous applications (Arshad 2009). In recent years, however, benefiting from the advancement in technology and the knowledge and inspiration gained from nature, engineers have started to develop biomimetic flow-sensors aimed at a high level of versatility, robustness and sensitivity.

Biomimetics or bionics strives to exploit the principles of natural systems and to implement them in engineering products using available or new technologies. Lately, the need for more advanced and robust systems and the biological discoveries of functional properties of organic systems have popularized this perspective among engineers (Vincent 2001).

Lateral line inspired flow-sensor arrays can be used to study hydrodynamic phenomena in complex, noisy environments. They provide invaluable means for the study of fluid mechanics especially of turbulent flow and can also potentially be used in Underwater Autonomous Vehicles (UAV) to increase manoeuvre efficiency (Arshad 2009).

¹ Hot-wire anemometers measure fluid velocity by detecting temperature changes of heated wires due to heat convection forced by fluid flow. However, their function is limited at low flow velocities due to their relatively low sensitivity.

² Laser Doppler velocimeters point a monochromatic laser beam towards a target and collect the reflected radiation. Due to the Doppler effect, the change in wavelength of the reflected radiation is a function of the relative velocity of the targeted object. They are usually complicated devices and need reflective particles. Moreover, sensors based on acoustic transmission and detection of Doppler phase shift are generally large.

³ Pressure distribution measurements can be used as an indirect way of flow sensing. However, information about the main stream is not accurately provided by this method.

2. Piezoresistive sensors

Piezoresistivity (Smith 1954) is a property of certain materials which change their electrical resistance when subject to tensile or compressive stresses. The effect is small in metal conductors but easily observable and exploitable in semiconductors such as silicon. It is a function of doping, temperature, crystallographic orientation, etc. Piezoresistive readout is commonly used to measure the deflection of members, such as cantilevers (see below) and membranes. It is possible to deduce the magnitude of force on a cantilever using piezoresistive regions (strain gauges) at the base, where the maximum stress occurs, by measuring resistance changes. These strain gauges are usually arranged in a Wheatstone bridge configuration and the change in resistance is proportional to the strain exerted on them. This relation is formulated as

$$\frac{\Delta R}{R} \propto \varepsilon \quad (1)$$

where R is the electrical resistance of the gauge, ΔR the change in R and ε the mechanical strain.

A *cantilever* is a beam that is fixed at one end and free at the other. Cantilevers at the micron-scale are made by micromachining, and have a wide range of applications in science and technology such as in AFM (Atomic Force Microscopy), chemical detection sensors, RF (Radio Frequency) filters and resonators, to name but a few. The basic principle of a cantilever-based sensor is

to determine the magnitude of a load from the amount of deflection. It has been shown (Gere 2003) that for a cantilever subjected to a transverse load, the maximum strain is at the base (fixed end) and is equal to

$$\varepsilon_{\max} = \frac{M \cdot c_1}{E \cdot I} \quad (2)$$

in which M is the magnitude of the developed moment at the base, E is the Young's modulus of elasticity, I is the second moment of area and c_1 is the distance from the neutral axis. For cantilevers made of an isotropic and homogeneous material $c_1 = t/2$ in which t is the thickness of the beam.

2.1 Sensors based on cantilevers

Fan et al. (2002) have realized a cantilever-based flow sensor with a piezoresistive readout mechanism. A PDMA⁴ process was utilized to obtain (820 μm long) out-of-plane cantilevers from in-plane fabricated cantilever beams. The fabrication starts with the selective doping of the silicon substrate with boron to form strain gauges. A backside etching process in alkaline (KOH) solution determines the cantilever's thickness. Thereafter, lead wires, a copper sacrificial layer and a thin gold layer, are deposited and patterned. Then Permalloy, which is necessary for the PDMA process, is electroplated. Subsequently, the cantilever is completed with an etching process on the front side. The sacrificial layer is removed in a wet etching process and, using a magnetic field, the Permalloy structure is raised to a permanent upright position. Finally a thin layer

⁴ Plastic Deformation Magnetic Assembly (PDMA) is a technique for three-dimensional assembly of micro structures. Certain parts of the structure can plastically deform by applying external magnetic fields which interact with the magnetic material deposited on the micro structure. The resultant force brings the entire structure to a certain angle at which the developed stress can surpass the elastic limit of material and cause permanent deformation. PDMA is a non-contact, batch process but it is relatively difficult to accurately control the deformation angles of the structures.

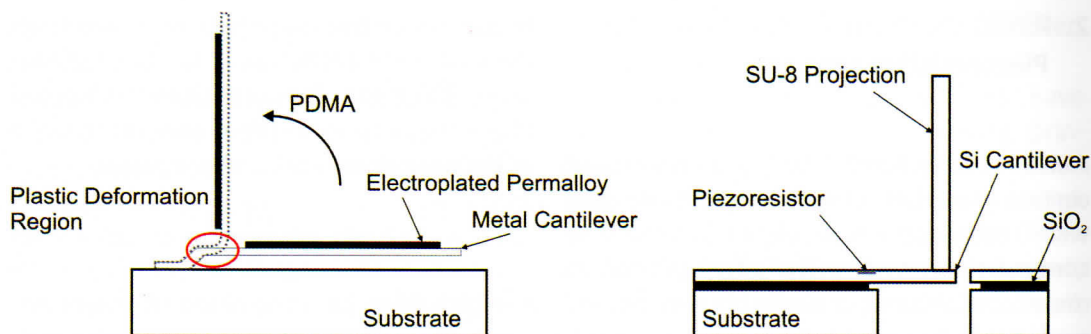


Fig. 1 Left: Schematic of cantilevers realised using PDMA (Fan et al. 2002, Chen et al. 2003). Right: Schematic of a SU-8 cylinder at the tip of a silicon cantilever (Yang et al. 2007)

of parylene is deposited in order to insulate the structure and the electrical conductors from water. The highest presented relative change of resistance, $\Delta R/R$, is 2.3×10^4 ppm at 1 m/s water flow speed.

The major advantage of this method is the monolithic fabrication process. However, according to the authors the robustness and compatibility of the device are a concern. The strength of the joint between out of plane and in plane cantilevers is crucial but it was shown that it is possible to strengthen the joint and define the exact bending point by electroplating a thin layer of gold.

In another approach Chen et al. (2003) employed the same PDMA principle and produced a polymer-based flow sensor. Their fabrication consists of successive metal and polymer deposition and patterning. The main difference is in the use of *NiCr* strain gauges on the base of polyimide film which forms the out-of-plane cantilever (600 to 1,500 μm long). Low temperature processing (the highest process tempera-

ture reported is 350 °C) allows the use of a variety of substrates including flexible polymer materials. Chen et al. (2003) also have claimed that this process is more robust and efficient than using silicon bulk and surface micromachining. However, the strain gauge efficiency is considerably lower. The sensor has been tested in air flow and the highest reported relative change of resistance, $\Delta R/R$, is 600 ppm at 10 m/s air flow speed.

Yang et al. (2007) have fabricated a cantilever-based flow sensor using SU-8⁵ polymer to produce a (500 μm long) cylindrical structure at the free end of a cantilever. The reported detection threshold⁶ amplitude is 0.1 mm/s at 25 Hz using 2 Hz FFT (Fast Fourier Transform) bandwidth⁷ (Chen et al., 2007) for measurements. The calculated resonance frequency is 1 kHz in water. The readout mechanism is the same as above, i.e. piezoresistive. The fabrication process begins with the use of Silicon On Isolator (SOI) wafers. Piezoresistive elements are then produced using ion implantation. Subsequently gold is

⁵ SU-8 is a photo-sensitive polymer used in MEMS technology. It can be spun with different thicknesses and is used for the fabrication of high aspect ratio structures.

⁶ Detection threshold is defined as the minimum detectable input. It depends on the properties of the sensor, the noise level and the measurement frequency resolution.

⁷ Using a narrow FFT bandwidth (low measurement resolution) reduces the (Gaussian) noise power incurred in the measurement and, therefore, increases the signal to noise ratio which results in a lower detection threshold. However, it increases the detection time.

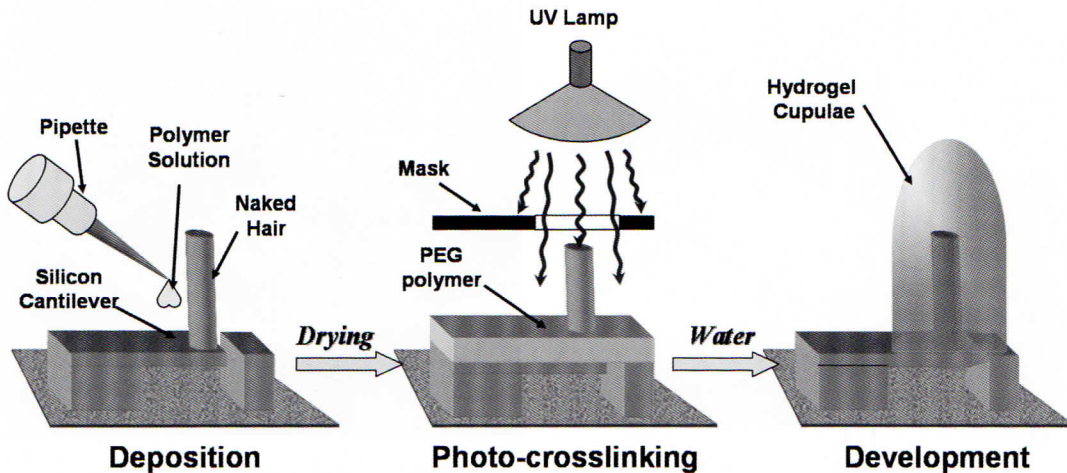
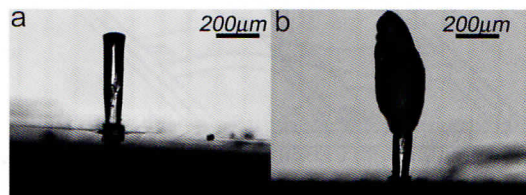


Fig. 2 Top: Schematic process steps to form a hydrogel cupula around the SU-8 hair at the tip of silicon cantilever (Peleshanko et al. 2007). Reproduced with permission of Wiley-VCH Verlag. **Right:** Microscopic pictures from a hair without **a** and with **b** hydrogel at the tip (McConny et al. 2009). Reproduced with permission of The Royal Society of Chemistry



deposited and patterned to form conductive wires and bond pads. This is followed by two DRIE⁸ steps, both on the front and backside of the wafer, to define the cantilever. Subsequently, SU-8 photoresist is spun and patterned to shape the hair-like extension and then the cantilever is immersed in BHF (Buffered Hydro-Fluoric acid) solution. The devices have been made in pairs oriented perpendicular to each other to provide flow measurement along two orthogonal axes. These sensors have a linear response to AC flow and the hair-like SU-8 structures can be deflected by up to 35° without degradation of performance. Using this sensor, Yang et al. (2010) have produced a lateral line system capable of flow source localisation in a 3D domain.

Peleshanko et al. (2007) have reported a 20 to 70 fold increase in sensitivity⁹ at frequencies between 10 to 110Hz, and a decrease in the detection threshold from 100 µm/s to 75 µm/s water flow speed of the previously mentioned sensor. A water soluble Polyethylene Glycol (PEG) is dispensed on the SU-8 cylinder (the hair) and its immediate surroundings. Then UV-photopolymerization is carried out to cross link the polymer around the hair. After this, the sensor is put into water so that non-cross-linked polymer is dissolved and the cross-linked polymer swells and forms a dome-shaped artificial cupula around the hair. The increase in sensitivity has been reasoned to be a result of 1) a larger drag force due to

⁸ Deep Reactive Ion Etching (DRIE) is a process to etch high aspect ratio structures in a silicon substrate.

⁹ The sensitivity is defined as the ratio of a change at output to the respective change at input. It is basically the slope of the calibration curve of the sensor.

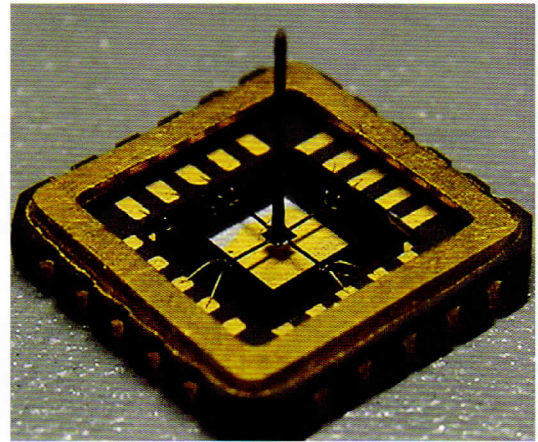
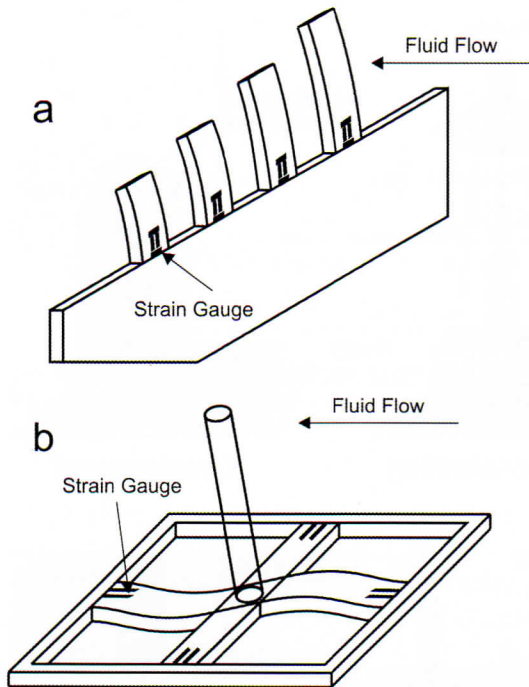


Fig. 3 Left: **a** In plane fabricated cantilevers are rotated to face the fluid flow. **b** A thin cylindrical wire is mounted at the joint of cross-shaped beams with piezoresistive elements at the base (Ozaki et al. 2000). Top: The hydrophone before packaging (Xue et al. 2007). Reproduced with permission of Elsevier

a larger effective cross section and 2) the coupling between the flow and the fluid trapped in the hydrogel (water content of the swallowed hydrogel is about 90 %). This approach also provides extra protection for the hair sensor. Using a similar principle, McConny et al. (2009) have reported a 38 fold increase in sensitivity and reduction of detection threshold to $2.5 \mu\text{m/s}$. In this approach the dispense process was modified to increase the length of the hair and its cross section at the top without changing the mechanical characteristics of the base of the hair. Although the fabrication process is not monolithic and, therefore, is not suitable for array fabrication, according to the authors, it rivals the fish mechanoreceptors in terms of sensitivity (see chapter 23 by McConny and Tsukruk).

Another attempt to mimic hair receptors was made by Ozaki et al. (2000). They suggested two types of structure: 1) The first structure is rather simple, and is basically a series of planar cantilevers with piezoresis-

tive strain gauges at the base. After fabrication the substrate is rotated by 90° to orient the cantilevers perpendicular to the direction of the fluid flow. The fabrication process is simple and very well developed in MEMS technology. The one dimensional nature of the fabricated array and its low density are two disadvantages of this approach. 2) The second configuration is a cross-shaped structure with a piezoresistive element at the end of each beam which is fixed to the substrate. A long metal wire is manually attached to the centre of the cross. This structure is made from thin ($200 \mu\text{m}$) silicon substrates which are first oxidized and patterned. Then Boron is diffused in order to make strain gauges. Anisotropic etching of the substrate from the backside in TMAH (TetraMethylAmmoniumHydroxide) is used to produce the beams. Afterwards aluminium interconnects are deposited and finally a Reactive Ion Etching (RIE) process from the front side is used to release the device. Although the fabrication process is simple, the

TMAH backside etching needs careful attention to accurately ensure the desired thickness. These structures have been made for and tested in air flow but potentially they can be used in water with minor modifications, mainly through the insulation of wires to prevent contact with water.

This second configuration has been repeated by Xue et al. (2007) and Zhang et al. (2008) who changed the piezo-transducer configuration and fabrication process and included external structures to adapt the sensor to aquatic environment. The hair is again attached manually. The sensor is connected to a 50 dB low noise preamplifier, immersed in Castor oil and protected using a Polychloroprene Rubber dome. The reported sensitivity is -197.7 dB (at 400 Hz) (0 dB = 1 V/ μ Pa).

Lee et al. (2006) use a piezoelectric polymer film or PVDF (Polyvinylidene Fluoride), which is bonded to the surface of aluminium cantilever beams. The overall size of the device in this approach is bigger (cantilevers are between 22 to 30 mm long) than the previous ones as macro-fabrication technology has been utilized. Therefore, their sensitivity and bandwidth are much lower compared to micro-fabricated counterparts.

2.2 All polymer sensors

Engel et al. (2006) have reported another type of hair-based flow sensor using Polyurethane elastomers and Force Sensitive Resistors (FSR). This consists of a hair-like structure on top of four FSRs which are in half bridge configuration and can reveal both magnitude and direction of displacement. When the structure deflects, the stress develops at its base and the resistance of the FSRs will change accordingly. The building process begins with the deposition and patterning of gold lead wires. Afterwards a thick photoresist is spun and patterned to form a mould for the FSRs. The actual FSRs are

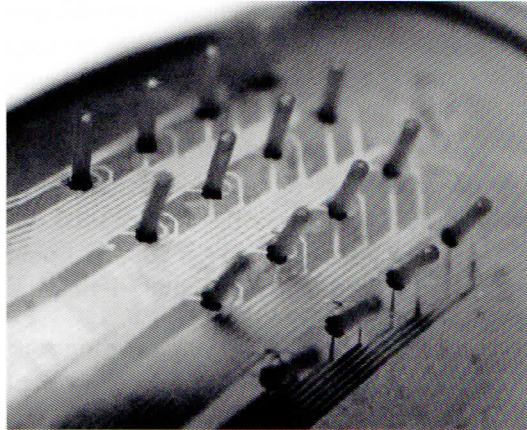


Fig. 4 Polyurethane hairs on flexible substrate (Engel et al. 2006). Copyright 2006 IEEE; reproduced with permission

made of polyurethane that is loaded with an electrical conductive filler. This filler can be Carbon Black (CB) or multiwall carbon nanotubes (MW-CNT). The FSR material is applied to the substrate and sacrificial photo resist is removed. The hairs are made by filling a wax mould with the polymer and are then aligned and attached to the FSR substrate. Subsequently, the wax mould is dissolved in hot water. These structures exhibit a great robustness but suffer from non-uniformity, viscoelastic creep, size and aspect ratio limitations (because the wax mould is formed by drilling) and cross-axis coupling (Engel et al. 2006). The latter can be partially overcome using optimized cross-sections.

2.3 Conclusion

The above mentioned sensors all use the piezoresistive effect as the readout mechanism. Piezoresistive readout has the advantage of being cheap and easy to fabricate. Moreover, the readout circuitry can be rather simple. The development of these sensors has already led to the production of artificial lateral line sensor arrays. However, piezore-

sistors are sensitive to temperature changes while the magnitude of change in resistance due to the stress is comparatively small with respect to the base resistance, i. e. the signal modulation is small. In addition, to decrease the thermal noise the base resistance needs to be small. When the base resistance decreases, the electrical current supply should increase to yield a strong signal, hence the power consumption increases.

3. **A capacitive sensor**

A capacitor consists of a pair of electrical conductors separated by an insulating material (dielectric). When a voltage difference is applied to the conductors an electric field is established in the dielectric material. Energy is stored in this electric field. The ability of a capacitor to store energy is characterised by its capacitance. An electrical capacitance C is defined as the ratio of the stored electric charge Q induced by establishing the electric potential V between the two electrodes. When these electrodes are parallel plate conductors it can be shown that¹⁰

$$C = \frac{\varepsilon \cdot A}{d} \quad (3)$$

is a physical characteristic of the configuration in which A is the overlapping area of the electrodes, d is the distance between them and ε is the electrical permittivity of the medium in between. A change of any of these three quantities is reflected in the magnitude of the capacitance and can be

measured with suitable electrical circuits. A capacitive sensor is a transducer which converts a stimulus to a corresponding change in a certain capacitance. A comprehensive study on the capacitive measurement principle can be found in de Jong (1994) and Baxter (1997).

A basic requirement for using capacitive readout in an aquatic environment is to prevent water from coming into contact with the electrodes. This may result in a short circuit or electrolysis if the water has sufficient conductivity. To overcome this difficulty conductors used in aquatic environments have to be insulated. In MEMS technology an option for achieving this is to deposit or spin a layer of a non-conductive polymer over the chip as mentioned in some of the previously noted devices. In addition, a capacitive change is usually due to a change in the distance of the two electrodes. Therefore the presence of a highly viscose medium in between the electrodes can degrade the performance of the device considerably¹¹ (Blech 1983).

3.1 Analysis and design

Figure 5 shows the concept of a capacitive aquatic hair-based flow sensor. A high aspect ratio¹² structure (the hair) is firmly attached to a fully supported membrane. The readout mechanism is beneath the membrane and is insulated from the fluid flow. This consists of two electrodes attached to the bottom side of the membrane and a common electrode at a distance below them. The configuration forms two capacitors, which can be used in a differential readout scheme reducing disturbing common mode signals such as

¹⁰ This is the case when the effect of the fringing electrical field is neglected, i.e. when the lateral dimensions of the electrodes are much larger than their separation gap.

¹¹ This effect is called squeeze film damping.

¹² Aspect ratio in this case is the ratio of the length of hair to its diameter.

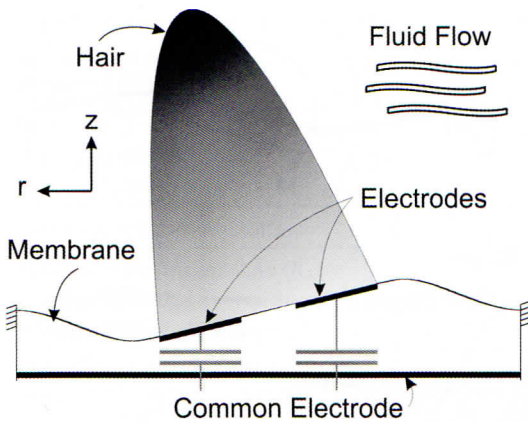


Fig. 5 Schematic view of a capacitive aquatic flow sensor. For clarity, the capacitances are shown by electrical symbols

changes in temperature, humidity, etc. Having the hair on a membrane forming a cavity devoid of water lessens the chances of short circuiting, prevents electrolysis and reduces squeeze film damping effects as discussed previously.

The hair deflects as a result of the drag force exerted by the fluid flow. This deflection is mirrored in the flexible membrane to which the hair is firmly attached. The distance between each of the electrodes and the common one, or in other words, the gap between the capacitor plates is then altered, as one gap increases while the other one decreases. By measuring the resulting change in capacitances, the amount of membrane and hair deflection, and hence the magnitude of the drag-force, thus the flow-velocity of the water can be deduced.

Geometrical optimization that takes into account technological possibilities and limitations is needed to ensure the realisation of a flow-sensor with the desired characteristics. To this end, a relation between the capacitance change and the flow velocity needs to be derived. This problem is divided into three parts and discussed in what follows.

3.1.1 On the magnitude of the force on the hair structure due to a specific flow velocity

The relation between an oscillatory fluid flow and the drag it exerts on a rotatable cylinder has been thoroughly dealt with in the literature, for example, in the context of the research on the principles of deflection of filiform hairs on cricket cerci and spider legs (see e.g. Shimozawa et al., 1998 and Humphrey and Barth, 2007). In brief, the fluid flow velocity profile close to the surface is determined first. Next, the hair structure is modelled as a rigid cylinder in a laminar flow and the drag force it incurs is calculated. To this end, the flow regime should be determined considering Reynolds and Strouhal numbers (Humphrey et al. 1993). Eventually, using a second order system approximation, the equation of motion is written as

$$I \frac{\partial^2 \theta_h}{\partial t^2} + R \frac{\partial \theta_h}{\partial t} + K_\phi \theta_h = \int_0^L F_s(z, t) \cdot z \cdot dz \quad (4)$$

in which L is the length of the hair, z is the distance from the substrate, F_s is the drag force and θ_h is the steady state response (the angle of deflection) of the system. The moment of inertia I is a result of the geometry of the structure with additional contributions due to fluid cylinder interaction. The damping coefficient R consists of the intrinsic structural damping and viscous damping of the fluid. In our sensor geometry, squeeze film damping needs to be added to this term. The torsional resistance K_ϕ depends on the mechanical characteristics of the structure and can be derived analytically.

3.1.2 On the deflection of the structure due to a specific torque

The right hand side of (4) is the torque that is generated by the drag force on the hair. It can be shown (Young and Budynas 2002) that for a fully supported plate with a trun-

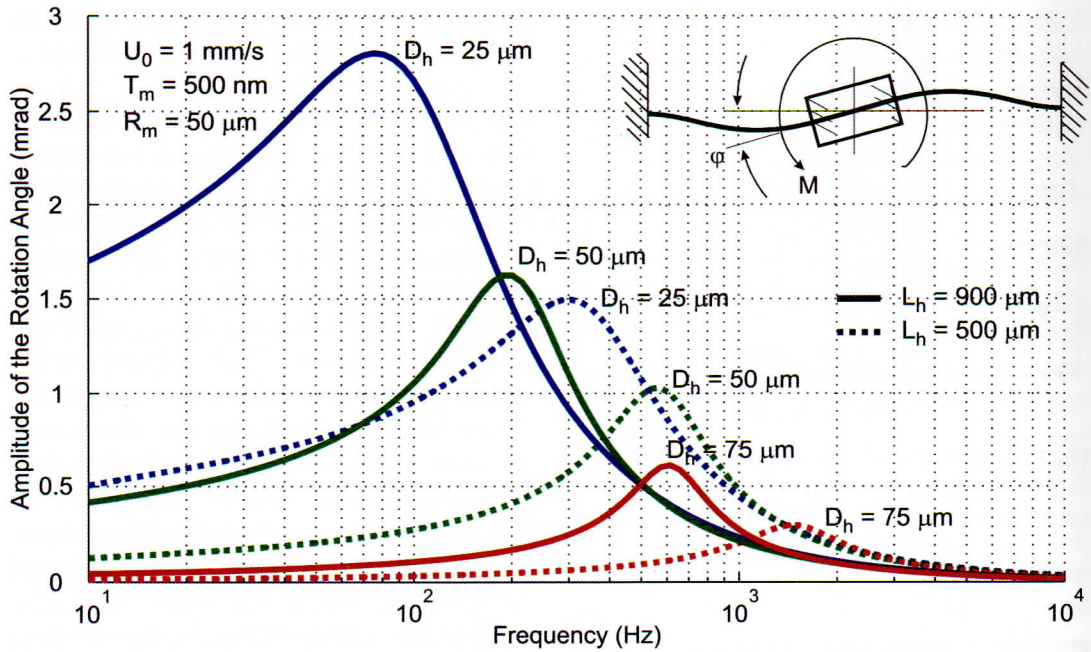


Fig. 6 Rotation angle as a function of frequency for different hair lengths and diameters. The inset shows the schematic view of the anti-symmetric deflection of a fully supported membrane

nion at the centre (Fig. 6, inset) the angle of deflection is related to the applied torque as

$$\varphi = \frac{\alpha(\zeta, \nu) \cdot M}{E \cdot T_m^3} \quad (5)$$

in which E is the Young's Modulus of elasticity, M is the torque acting on the hair, T_m is the membrane thickness and $\alpha(\zeta, \nu)$ is a constant which depends on Poisson's ratio ν and the ratio of the diameters of the trunnion (R_h) and the membrane (R_m). For $\zeta = R_h/R_m = 0.5$ and $\nu = 0.3$, it is derived that $\alpha = 0.081$ (Timoshenko and Woinowsky-Krieger 1959). It is intuitively clear that for a specific thickness of the membrane the flexibility increases as the ζ ratio decreases. However, the fabrication of thin hairs and large membranes has some limitations. In addition, the drag force on a thin hair is relatively small. Figure 6 shows the deflection of a 500 nm thin SU-8 membrane.

The stiffness of the membrane is also affected by its shape. The above calculations

have been made based on the use of a circular membrane. However, it can be shown that an elliptical membrane with its major axis along the desired direction of measurement shows a larger deflection than a circular one for given torque. For these membranes an additional design parameter that should be taken into consideration is the ratio of the semi-major to semi-minor axes.

3.1.3 On the relative capacitance change due to a specific deflection angle of the hair structure

The capacitance depends on the area and the shape of electrodes. At the initial state (no deflection) the capacitance is easily obtained using (3). To calculate the capacitance while the membrane is deflected, C_f , we need to evaluate

$$C_f = \int \int \frac{\varepsilon}{d_0 + w(r, \theta)} \cdot r \cdot dr \cdot d\theta \quad (6)$$

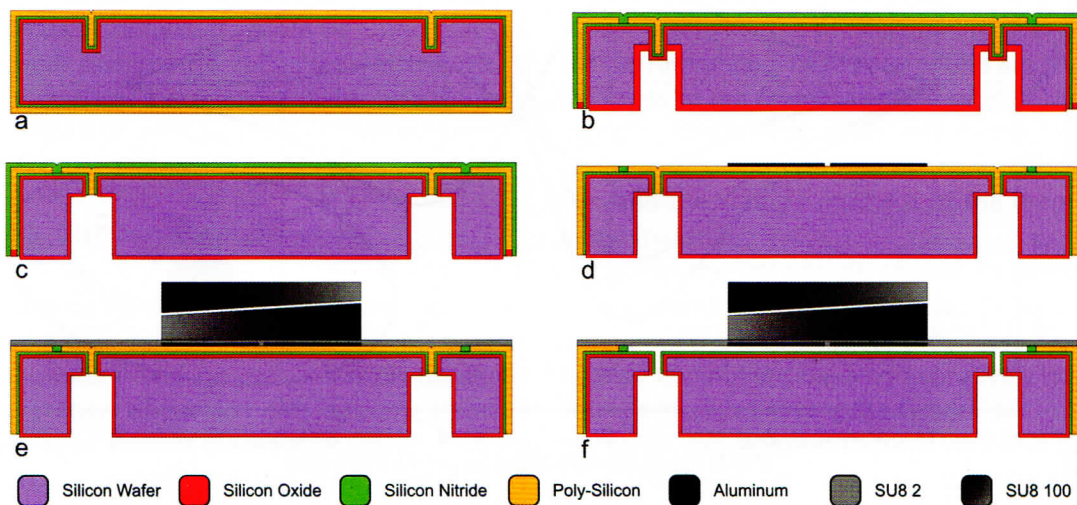
Table 1 The design parameters and resulting characteristics of the sensor

| Material (SU-8) | | Material (Water) | |
|---|-------------------------|--|---------------------------------|
| Density | 1 200 kg/m ³ | Density | 1 000 kg/m ³ |
| Young's Modulus (E) | 4.4 GPa | Dynamic Viscosity | 1.002 × 10 ⁻³ Pa · s |
| Poisson's Ratio | 0.22 | Speed of Sound | 1 500 m/s |
| Geometrical Dimensions | | | |
| Radius of the membrane (R _m) | 50 μm | Length of the hair (L _h) | ~900 μm |
| Thickness of the membrane (T _m) | ~500 nm | Initial gap between electrodes (d ₀) | ~1 μm |
| Radius of the hair (R _h) | ~25 μm | | |
| Characteristics (calculated) | | | |
| Resonance Frequency | ~200 Hz | Detection Threshold | ~2.2 mm/s at 100 Hz |
| Quality Factor | ~1 | Sensitivity | ~154 fF/mm/s at 100 Hz |

in which r and θ denote the polar coordinates, d_0 is the initial gap between the electrodes and $w(r, \theta)$ is the analytical solution for the deflection of the membrane. This integral needs to be solved numerically. The more exact measure can be obtained using Finite Element Analysis (FEA). Table 1 above summarises the design parameters, geometrical dimensions and the resulting characteristics of the sensor.

3.2 Fabrication

The fabrication process has been thoroughly described in Izadi et al. (2010) and is schematically shown in Fig. 7. It starts with a highly doped silicon wafer (which acts as a common electrode). At the first step a DRIE process is used to make 60 μm deep and 4 μm wide trenches (etch ports) on the front side of the wafer. This is followed by an oxidation process and the deposition of a stoichiometric silicon nitride (Si₃N₄) layer. Subsequently, polysilicon is deposited to close the

**Fig. 7** Abridged fabrication process

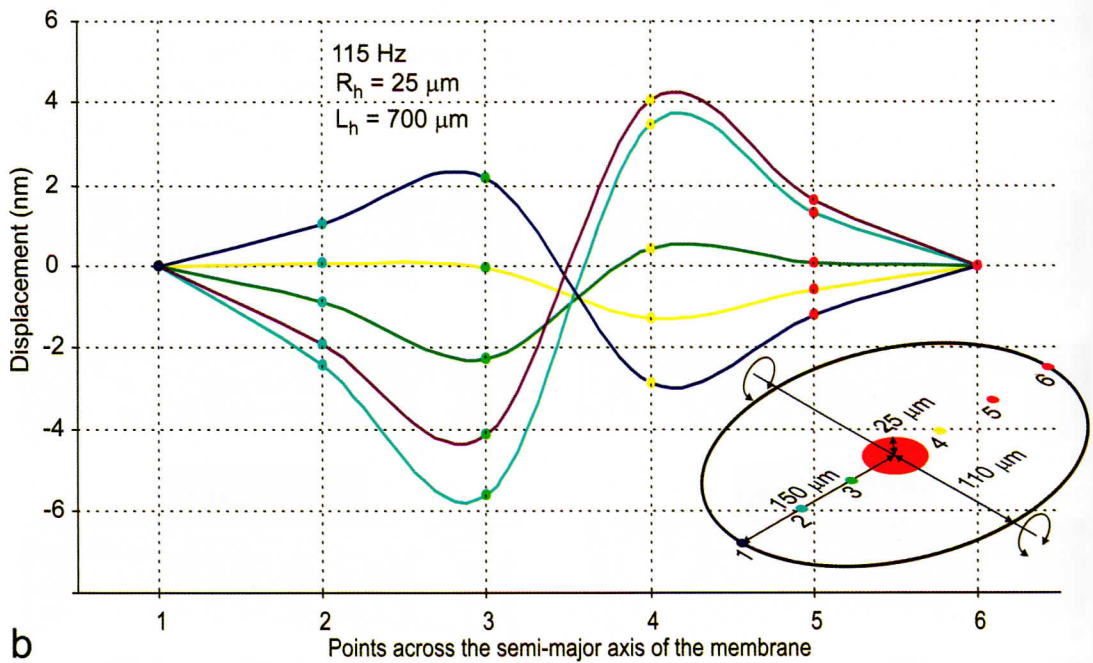
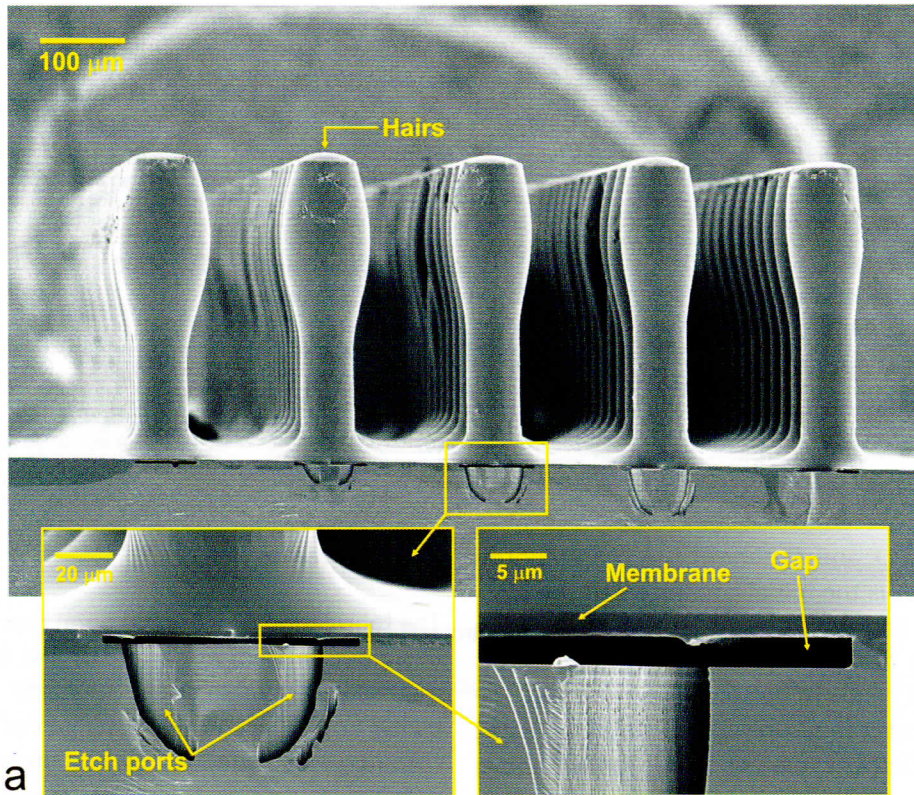


Fig. 8 **a** SEM picture of capacitive hair based flow sensor. **b** Displacement of an elliptical membrane measured across its semi-major axis with laser vibrometer in air

etch port openings. Therefore, the minimum thickness of the polysilicon layer is determined by the width of the etch ports, and the thickness determines the gap between the electrodes. To define membranes, a rim is etched and re-filled with Silicon Rich silicon Nitride (SiRN). After a back-side DRIE step and wet oxidation, a directional SF_6 based plasma with enhanced ion bombardment is used to open the protection stack at the etch ports and expose the sacrificial polysilicon layer. Then, the SiRN layer is removed from the front side and low stress aluminium electrodes are deposited. A thin layer (~ 500 nm) of SU-8 is spun and selectively exposed to form the membranes. This is followed by a thick SU-8 (500 to 800 μ m) spin, exposure and development step to form the hairs. The shape of the hairs, using the negative tone properties of SU-8, is tuned to increase the drag force on them by increasing the diameter at the top. Finally, using a selective SF_6 based high density plasma without self bias, the sacrificial layer is etched to release the membranes (see Fig. 8a).

Using a laser vibrometer, preliminary mechanical tests of the fabricated sensor have been made in air. At the right side of Fig. 8 the displacement of an elliptical membrane in the half cycle of oscillation at different phases is shown. It should be noted that the small asymmetric deflections of the membranes are a result of a slight misalignment of the hair relative to the membrane.

3.3 Distributed sensory array

Although a single sensor may be capable of fluid flow detection, the full functionality of the lateral line systems relies on the interpretation of parallel data streams from an array of sensors (Casas et al. 2010). Such an array provides both spatially and temporally rich data that can be used to construct a 3D map of the immediate environment. Fortu-

nately, MEMS technology enables us to fabricate arrays, as can be seen in Fig. 8. The fabrication of hairs with different diameters can be carried out in a single lithography step. Various hair lengths can be achieved using multiple SU-8 patterning processes. However, as the number of layers increases the processing becomes more difficult. The differences in diameter and length translate directly into variations in frequency characteristics. The result is that the sensor dynamic range and frequency response are widened.

The distance of the hairs along the stream of flow is another important design parameter. The boundary layer and wake beyond a hair can have a substantial effect on the drag force on the next hair. This phenomenon is called viscous coupling and theories have been developed to predict and control it (Bathellier et al. 2005, Cummins et al. 2007).

3.4 Discussion

The performance of the sensor has at least two dimensions: the sensitivity and the bandwidth. Evaluation of the collective influence of geometrical dimensions and material properties on these characteristics of the sensor highlights the decisive parameters in the performance. These parameters are the thickness of the membrane, the ratio of the hair diameter to that of the membrane, denoted by ζ , the length and diameter of the hair and the Young's modulus of the membrane material.

Clearly, the membrane should be made of a compliant material with low Young's modulus. SU-8 is compatible with micro-fabrication technology, has a comparatively low Young's modulus among the typical "MEMS" materials, can be spun to form very thin or very thick layers and is a photo structurable polymer, hence a reasonable choice for both membrane and hair. To obtain a lower tor-

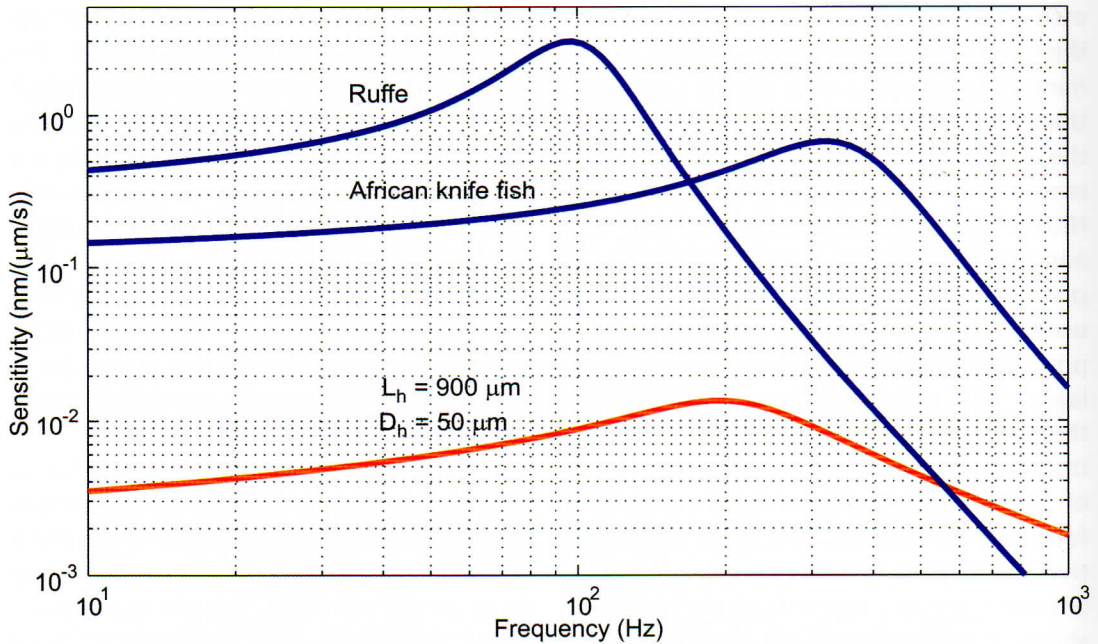


Fig. 9 Comparison of the mechanical sensitivities of the capacitive sensor and fish neuromast

sional stiffness, ζ should be small, thus the membrane area should be large and the hair should be thin. However, a membrane with a large area is more difficult to produce and is more susceptible to stiction. At the same time, a thin hair experiences less drag. Therefore, these parameters should be optimised to yield the highest sensitivity for a desirable bandwidth. On the other hand, the aspect ratio of the hair, i.e. length to diameter ratio, is technologically limited; the thinner the hair, the shorter it is. Therefore, the length of the hair, which should be maximised, is also linked to its diameter. Note that a thin, long hair has advantage over a short, thick hair even when ζ is constant. It can be shown that when the membrane radius is $50\ \mu\text{m}$, considering an aspect ratio of 20, the highest sensitivity is achieved with a hair diameter between 20 to $25\ \mu\text{m}$.

The thickness of the membrane has the greatest effect on the performance of the

sensor and should be minimised. Using SU-8, the minimum achievable thickness of a defect free membrane is around $400\ \text{nm}$. The use of other materials, for example, Parylene, which can be deposited in even thinner layers, e.g. $100\ \text{nm}$, potentially leads to a more sensitive sensor.

In short, to achieve higher sensitivity the hair should be long, the membrane thin and flexible and ζ should be small. The excessive downward deflection due to the static hydrostatic pressure across a thin membrane can be avoided by adjusting the pressure of the back chamber. In the frequency and amplitude range of interest, the resultant increase of the squeeze film damping due to the higher pressure does not affect the dynamic behaviour of the system.

The mechanical sensitivity of the sensor, defined as the mean displacement of one electrode per unit flow velocity, is shown in Fig. 9 and compared with that of fish¹³ (van

¹³ The sensitivity of fish has been defined as the neuromast displacement per unit flow velocity.

Netten 2006). It is seen that using the proposed geometry and materials, the sensitivity of the sensor is around two orders of magnitude below its natural counterpart. In order to achieve a higher sensitivity, as discussed above, the drag pickup mechanism should be further improved and a thinner, larger and hence more flexible membrane should be employed. Furthermore, the overall performance is affected by the electrical sensitivity which is determined by the parasitic capacitances and the minimum detectable relative change of capacitance, $\Delta C/C$, both of which should be reduced by improvement of the readout circuit or possibly by integration of it with the sensor.

3.5 Conclusion

Inspired by the function of the neuromast organ of the lateral line system, a hair-based aquatic flow velocity sensor and its fabrication process have been proposed. Capacitive sensing is chosen as the readout mechanism as it offers accuracy, high resolution and low power consumption. However, several difficulties arise from using the capacitive sensing principle in a conductive medium with high density and viscosity, like water. These stem mainly from the electrical insulation of the electrodes (to prevent electrolysis and short circuit), added inertia of the movable electrodes and squeeze film damping. The result is a rather complicated, but feasible, fabrication process.

Summary

The research covering different sensory organs of animals is a rich field. Evolutionary pressure forces virtually each part of a living creature to adapt to the organisms' environmental conditions to ensure survival and reproduction. Biological studies of sensory organs reveal solutions emerging from nature that provide vital information for an animal. Recently attention and effort of engineers has been drawn to mim-

ic nature's blueprints and to fabricate artificial counterparts of these sensory organs with the aim of reaching a higher level of performance and robustness necessary in modern technological applications.

The lateral line of fish has received great attention in recent years, and we have briefly reviewed here some of the efforts to mimic this system and to detail the design and fabrication of a capacitive sensor approach which promises great sensitivity and low power consumption. The most powerful feature of the lateral line is its property as an array. This enables fish to construct a 3D view of their environment, rather than just having a means for velocity measurement, and enables them to navigate in murky water or even if they are blind. MEMS technology provides us with the ability to fabricate large sensor arrays in monolithic processes. These artificial sensors will benefit the study of fluid dynamics and the study of aquatic animal behaviour, and are key to improving the performance of underwater robotic systems.

References

- Arshad MR (2009) Recent advancement in sensor technology for underwater applications. *Indian J Mar Sci* 38: 267–273
- Bathellier B, Barth FG, Albert JT, Humphrey JAC (2005) Viscosity-mediated motion coupling between pairs of trichobothria on the leg of the spider *Cupiennius salei*. *J Comp Physiol A* 191: 733–746
- Baxter LK (1997) Capacitive sensors: design and application. IEEE Press series on Electronics Technology
- Blech JJ (1983) On isothermal squeeze films. *J Lubr Technol* 105: 615–620
- Casas J, Steinmann T, Krijnen G (2010) Why do insects have such a high density of flow-sensing hairs? Insights from the hydromechanics of biomimetic MEMS sensors. *J R Soc Interface*, doi: 10.1098/rsif.2010.0093
- Chen J, Engel JM, Liu C (2003) Development of polymer-based haircell using surface micromachining and 3D assembly. In: Proceedings of the 12th International Conference on Solid State Sensors, Actuators and Microsystems, Transducer 2003, Boston, pp 1035–1038
- Chen J, Liu C (2003) Development and characteri-

- zation of surface micromachined out-of-plane hot-wire anemometer. *IEEE ASME J Microelectromech Syst* 12: 979–988
- Chen N, Tucker C, Engel JM, Yang YC, Pandya S, Liu C (2007) Design and characterization of artificial haircell sensor for flow sensing with ultrahigh velocity and angular sensitivity. *IEEE ASME J Microelectromech Syst* 16: 999–1014.
- Coombs S (2001) Smart skins: information processing by lateral line flow sensors. *Autonomous Robots* 11: 255–261
- Cummins B, Gedeon T, Klapper I, Cortez R (2007) Interaction between arthropod filiform hairs in a fluid environment. *J Theor Biol* 247: 266–280
- de Jong JW (1994) Smart capacitive sensors. Delft University press, Delft
- Dijkgraaf S (1963) The functioning and significance of the lateral-line organs. *Biol Rev* 38: 51–105
- Engel JM, Chen J, Liu C, Bullen D (2006) Polyurethane rubber all-polymer artificial hair cell sensor. *IEEE ASME J Microelectromech Syst* 15: 729–736
- Fan Z, Chen J, Zou J, Bullen D, Liu C, Delcomyn F (2002) Design and fabrication of artificial lateral line flow sensors. *J Micromech Microeng* 12: 655–661
- Fernandez VI, Hou SM, Hover FS, Lang JH, Triantafyllou MS (2007) Lateral line inspired MEMS-array pressure sensing for passive underwater navigation. In: *Proceedings of the International Symposium on Unmanned Untethered Submersible Technology, UUST 2007*, Autonomous Undersea Systems Institute
- Gere JM (2003) *Mechanics of materials*, 6th edn. Thompson-Engineering
- Humphrey JAC, Barth FG (2008) Medium flow-sensing hairs: biomechanics and models. In: Casas J, Simpson SJ (eds) *Advances in insect physiology. Insect mechanics and control*, Vol. 34, Elsevier Ltd, pp 1–80
- Humphrey JAC, Devarakonda R, Iglesias I, Barth FG (1993) Dynamics of arthropod filiform hairs. I. Mathematical modelling of the hair and air motions. *Phil Trans R Soc Lond B* 340: 423–444
- Izadi N, de Boer MJ, Berenschot JW, Krijnen GJM (2010) Fabrication of superficial neuromast inspired capacitive flow sensors. *J Micromech Microeng* 20: 085041
- Jentink HW, van Beurden JAJ, Helsdingen MA, Mul FFM, Suichies HE, Aarnoudse JG, Greve J (1987) A compact differential laser Doppler velocimeter using a semiconductor laser. *J Phys E: Sci Instrum* 20: 1281–1283
- Krijnen GJM, Floris J, Dijkstra MA, Lammerink TSJ, Wiegerink RJ (2007) Biomimetic micromechanical adaptive flow-sensor arrays. In: *Proc SPIE Europe Microtechnologies for the New Millennium*, Maspalomas, Gran Canaria, Spain, pp 6592–6608
- Lee YS, Im HJ, Kwon J, Yoon DJ (2006) Biologically inspired smart sensor for acoustic emission detection. *Key Eng Mater* 321–323: 204–207
- Leydig F (1850) Über die Schleimkanäle der Knochenfische. *Arch Anat Physiol Wiss Med*: 170–181
- McConney ME, Chen N, Lu D, Hu HA, Coombs S, Liu C, Tsukruk VV (2009) Biologically inspired design of hydrogel-capped hair sensors for enhanced underwater flow detection. *Soft Matter* 5: 292–295
- Ozaki Y, Ohyama T, Yasuda T, Shimoyama I (2000) Air flow sensor modelled on wind receptor hairs of insects. In: *Proc IEEE 13th International Conference on Micro Electro Mechanical Systems, MEMS 2000*, Miyazaki, Japan, pp 531–536
- Peleshanko S, Julian MD, Ornatska M, McConney ME, LeMieux MC, Chen N, Tucker C, Yang Y, Liu C, Humphrey JAC, Tsukruk VV (2007) Hydrogel-encapsulated microfabricated haircells mimicking fish cupula neuromast. *Adv Mater* 19: 2903–2909
- Shimozawa T, Kumagai T, Baba Y (1998) Structural scaling and functional design of the cercal wind-receptor hairs of cricket. *J Comp Physiol A* 183: 171–186
- Smith CS (1954) Piezoresistance effect in germanium and silicon. *Phys Rev* 94: 42–49
- Timoshenko S, Woinowsky-Krieger S (1959) *Theory of plates and shells*, 2nd edn. McGraw-Hill
- van Netten SM (2006) Hydrodynamic detection by cupulae in a lateral line canal: functional relations between physics and physiology. *Biol Cybern* 94: 67–85
- Vincent JFV (2001) Stealing ideas from nature. In: Pellegrino S (ed) *Deployable structures*. Springer, Vienna, pp 51–58
- Voigt R, Carton AG, Montgomery JC (2000) Responses of anterior lateral line afferent neurons to water flow. *J Exp Biol* 203: 2495–2502
- von Campenhausen C, Riess I, Weissert R (1981) Detection of stationary objects by the blind cave fish *Anoptichthys jordani* (Characidae). *J Comp Physiol A* 143: 369–374
- Xue C, Chen S, Zhang W, Zhang B, Zhang G, Qiao H (2007) Design, fabrication and preliminary char-

- acterization of a novel MEMS bionic vector hydrophone. *Microelectron J* 38: 1021–1026
- Yang Y, Chen N, Tucker C, Engel JM, Pandya S, Liu C (2007) From artificial hair cell sensor to artificial lateral line system: development and application. In: *Proc IEEE 20th International Conference on Micro Electro Mechanical Systems, MEMS 2007, Kobe, Japan*, pp577–580
- Yang Y, Nguyen N, Chen N, Lockwood M, Tucker C, Hu H, Bleckmann H, Liu C, Jones DL (2010) Artificial lateral line with biomimetic neuromasts to emulate fish sensing. *Bioinspir Biomim* 5: 016001
- Young WC, Budynas RG (2002) *Roark's formulas for stress and strain*, 7th edn. McGraw-Hill Education-Europe
- Zhang B, Qiao H, Chen S, Liu J, Zhang W, Xiong J, Xue C, Zhang G (2008) Modelling and characterization of a micromachined artificial hair cell vector hydrophone. *Microsyst Technol* 14: 821–828

Friedrich G. Barth · Joseph A. C. Humphrey

Mandyam V. Srinivasan *Eds.*


Frontiers in Sensing

Biological sensory systems, fine-tuned to their specific tasks with remarkable perfection, have an enormous potential for technical, industrial, and medical applications. This applies to sensors specialized for a wide range of energy forms such as optical, mechanical, electrical, and magnetic, to name just a few.

This book brings together first-hand knowledge from the frontiers of different fields of research in sensing. It aims to promote the interaction between biologists, engineers, physicists, and mathematicians and to pave the way for innovative lines of research and cross-disciplinary approaches. The topics presented cover a broad spectrum ranging from energy transformation and transduction processes in animal sensing systems to the fabrication and application of bio-inspired synthetic sensor arrays. The various contributions are linked by the similarity of what sensing has to accomplish in both biology and engineering.

ISBN 978-3-211-99748-2



 springer.at